

Synthesis, crystal structure, *in-silico* ADMET, molecular docking and dynamics simulation studies of thiophene-chalcone analogues

S. Nanjundaswamy^a, Gurumallappa^a, M.K. Hema^b, C.S. Karthik^{a,*},
Jothi Ramalingam Rajabathar^c, Selvaraj Arokiyaraj^d, N.K. Lokanath^b, P. Mallu^{a,*}

^a Department of Chemistry, SJCE, JSS Science and Technology University, Mysuru, Karnataka 570 006, India

^b Department of Studies in Physics, University of Mysore, Manasagangotri, Mysuru, Karnataka 570 006, India

^c Department of Chemistry, King Saud University, P.O. Box.2455, Riyadh 11451, Saudi Arabia

^d Department of Food Science and Biotechnology, Sejong University, South Korea

ARTICLE INFO

Article history:

Received 1 May 2021

Revised 15 July 2021

Accepted 22 August 2021

Available online 25 August 2021

Keywords:

Antibacterial agent

Chalcone

Thiophene

Molecular docking and MD simulations

ABSTRACT

A novel thiophene-based chalcone derivatives, 3-(pyridin-4-yl)-1-(thiophen-2-yl)prop-2-en-1-one (Compound 1) and 3-mesityl-1-(thiophen-2-yl)prop-2-en-1-one (Compound 2) were synthesized and single crystals were grown using slow evaporation technique. The structure of the synthesized compound was confirmed using mass spectroscopy, ¹H-NMR and FTIR spectroscopy. Single crystal X-ray structural analysis reveals that both crystals are crystallized under a monoclinic P21/n space group. C-H...O, C-H...Pi and Pi...Pi intra and intermolecular hydrogen bond interactions of compound 1 and C18-H18C...O7 (2.638 Å) and C3-H3...S1 (2.915 Å) intermolecular interactions in compound 2 contributed to molecular stability. The thiophene-chalcones analogues were screened for the *in-silico* studies to understand the antibacterial activity. Molecular docking study was analyzed for the compound 1 and 2 with Penicillin binding proteins (PDB:1MWT) and *Staphylocoagulase* (PDB:1NU7) of MRSA. Compound 1 showed -6.0 kcal/mol for both Penicillin binding proteins and *Staphylocoagulase* while compound 2 showed the binding score -6.9 kcal/mol for 1MWT and -7.1 kcal/mol for 1NU7 protein, respectively. The crystallized compounds were also examined for their ADMET analysis and it was observed that there was no AMES toxicity in both compounds. Compound 1 and 2 were also showed 0.529 log mg/kg/day and 1.096 log mg/kg/day maximum tolerated dose (human), respectively. Ultimately, molecular dynamics simulation of compound 1 and 2 confirmed the best possible interaction and stability in the active site of 1NU7 and allosteric site of 1MWT proteins for 20 ns.

© 2021 Elsevier B.V. All rights reserved.

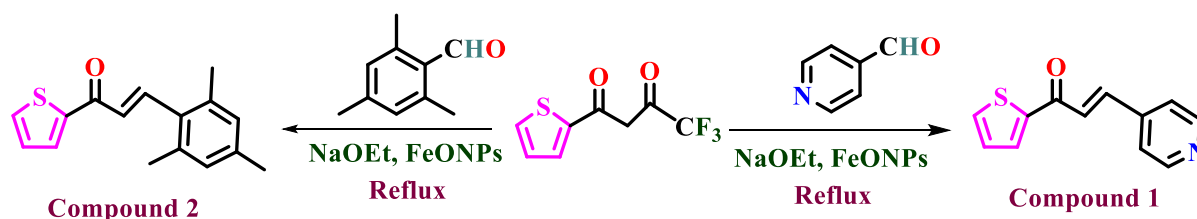
1. Introduction

Chalcones (1,3-diphenylprop-2-ene-1) are a group of organic compounds that comprise two aromatic rings, associated with an unsaturated ketone moiety [1,2]. Chalcones are a key group containing electron donors, acceptors groups attached to aromatic rings in various positions, that lead to change the properties of the molecules [3]. To transform them into remarkable compounds based on the formation of carbon-carbon bonds, various methods like Claisen-Schmidt condensation [4], grinding process [5], Suzuki coupling reaction [6], microwave irradiation [7], and Friedel-Crafts acylation [8] can be used. Chalcones are now considered as promising lead compounds in a wide range of pharmaceutical and medicinal chemistry applications due to their in-

teresting biological activity and their versatile nature of flexible structure [9,10]. Natural and synthetic chalcones provide a broad variety of antimicrobial [11], anti-inflammatory [12], anticancer [13] and antioxidant [14] properties towards human diseases. Of late chalcones with heteroatoms have gained interest; especially those with thiophene substituents have gotten attracted global interest. Several researchers have documented chalcones with heteroatoms such as halogens, Sulphur and Nitrogen atoms, particularly thiophene containing chalcones are reported due to their several applications, such as antimicrobial [15], antibacterial [16], antifungal [17], anti-inflammatory [18], and antimalarial [19] function. Researchers have been interested in organic single crystals due to their extremely sustained orientation stability and high density of active components, as evidenced in existing literature [20]. Infor cites of above-mentioned properties structural analysis of crystals about to bonding properties of the atoms in a molecule, crystal symmetry, hydrogen bond interaction and crystal packing properties are evaluated by using single crystal X-ray diffraction tech-

* Corresponding authors.

E-mail addresses: nanjundaswamy.s144@gmail.com (S. Nanjundaswamy), csk@jssstuniv.in (C.S. Karthik), drmallu66@gmail.com (P. Mallu).



Scheme 1. Schematic representation of synthesis of title compounds.

nique. The application of computational approaches to the evaluation of antibacterial activities against Methicillin-resistant *Staphylococcus aureus* (MRSA) has shown tremendously useful in understanding the structures and other essential physicochemical properties.

The present research work demonstrates the synthesis, characterization, molecular docking and dynamic simulation studies of novel thiophene-based chalcone derivatives. Single crystal X-ray structural investigation leads to the identification of various intermolecular interactions which contribute to the protein-ligand binding. Molecular docking studies revealed good binding scores of novel compounds with the 1MWT and 1NU7 proteins of MRSA bacteria and these docking results were best validated by the molecular dynamic simulation studies.

1.1. Materials and method

High purity chemicals and reagents were purchased from Sigma Aldrich (Merck Pvt. Ltd., India). The elemental analysis was obtained from Perkin Elmer 2400 elemental analyzer. The FT-IR spectra were recorded on a Perkin Elmer Spectrum Version 10.03.09. The ^1H NMR spectra (Agilent-NMR) were recorded using CDCl_3 as solvent at 400 MHz. Chemical shifts were reported in parts per million relative to TMS. A water micro TOF QII mass spectrometer was used to determine the mass of the synthesized compounds.

1.2. Synthesis of thiophene chalcones

A mixture of 4,4,4-trifluoro-1-(thiophen-2-yl)butane-1,3-dione (1 equivalence) and aldehydes (1 equivalence) was dissolved in ethanol, catalytic amount of sodium ethoxide and FeONPs were added. The reaction mixture was refluxed for 5–6 h. The completion of the reaction was espied by thin layer chromatography. After the completion of the reaction, the reaction mixture was filtered and poured into crushed ice, the separated solids were filtered and recrystallized from ethanol. The synthesis of thiophene chalcones is outlined in Scheme 1.

1.2.1. Compound 1. 3-(pyridin-4-yl)-1-(thiophen-2-yl)prop-2-en-1-one

FT-IR (KBr, cm^{-1}): 1654 (C=O), 1588 (C=C), 1418 (Ar, C=C), 720 (C-S). ^1H NMR: (400 MHz, CDCl_3) 8.72 (d, 2H, Py-H), 7.98 (d, 1H, Ar-H), 7.80 (d, 1H, Ar-H), 7.68 (d, 1H, CH=C), 7.53 (d, 2H, Py-H), 7.11 (t, 1H, Ar-H), 7.00 (d, 1H, C=CH). ^{13}C : (400 MHz, CDCl_3) 180.33, 154.75, 148.81, 143.45, 139.71, 137.02, 132.81, 130.17, 129.05, 127.07, 124.37, 122.74. MS (ESI) m/z: 215.04. Elemental Analysis: Calculated: For $\text{C}_{12}\text{H}_9\text{NOS}$ (in %): C-66.95, H-4.21, N-6.51. Found: C-66.87, H-4.37, N-6.40.

1.2.2. Compound 2. 3-mesityl-1-(thiophen-2-yl)prop-2-en-1-one

FT-IR (KBr, cm^{-1}): 1647 (C=O), 1592 (C=C), 1413 (Ar, C=C), 716 (C-S). ^1H NMR: (400 MHz, CDCl_3) 7.88 (d, Th-H, 1H), 7.82 (d, Th-H, 1H), 7.72 (d, C=CH, 1H), 7.21 (t, Th-H, 1H), 6.92 (s, Ar-H, 2H), 6.73 (d, C=CH, 1H), 2.44 (s, CH_3 , 3H), 2.32 (s, CH_3 , 3H), 2.14 (s, CH_3 , 3H). ^{13}C : (400 MHz, CDCl_3) 180.31, 145.12, 139.74, 137.42,

134.66, 132.83, 130.16, 129.02, 127.86, 121.32, 21.93, 19.84. MS (ESI) m/z: 256.09. Elemental Analysis: Calculated: For $\text{C}_{16}\text{H}_{16}\text{SO}$ (in %): C-74.96, H-6.29. found: C-74.53, H-6.09.

2. Experimental

2.1. Single crystal X-ray structure determination

Single crystal X-ray intensity data were collected at 293 K using graphite-monochromated Mo- $\text{K}\alpha$ ($\lambda=0.71073 \text{ \AA}$) radiation equipped with Rigaku XtaLAB mini three-circle CCD diffractometer. The data was collected with an exposure time of 3s and the scan width of 1° . The data collection strategy was planned and executed using CrystalClear-SM Expert 2 [21]. Structure solution was carried out using direct methods and refinement by full-matrix least-squares against F^2 using SHELXS and SHELXL-2018 [22,23] programs as implemented in OLEX2 software [24]. The non-hydrogen atoms were assigned with anisotropic displacement parameters. Crystal structure geometry calculations were carried out using the PLATON program [25]. The ORTEP and packing diagram of both compound 1 and 2 was generated using MERCURY4.2.0 [26]. The complete crystallographic data and refinement parameters are summarized in Table 1.

2.2. Molecular docking

Molecular docking studies were carried out using Auto-Dock Vina 1.5.6 tool. It was used to demonstrate feasible docking modes of interaction between ligand and biological targets of interest. The 3D structure of the target protein was obtained in the PDB format from the RCSB Protein Data Bank (PDB ID: 1NU7 & 1MWT). The bounded ligand was removed by using Biovia Discovery Studio 2019. The energy of proteins was reduced using an Auto-Dock method and polar hydrogen atoms were added [27]. In order to identify the binding sites, the grid box was built using the grid size of $X = 17.71$, $Y = 55.99$, $Z = 44.36$ for *Staphylocoagulase* and $X = 13.33$, $Y = 30.36$, $Z = 23.67$ for PBP2a allosteric site. The 3D structure of the compound was saved in PDB format with the Marvin JS program. The binding affinity of the ligand with a unit of kcal/mol was noted as a negative ranking. Using Biovia Discovery Studio 2019, the protein-ligand interactions were analyzed and visualized.

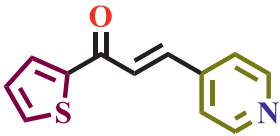
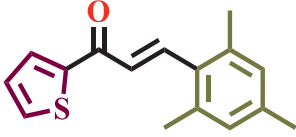
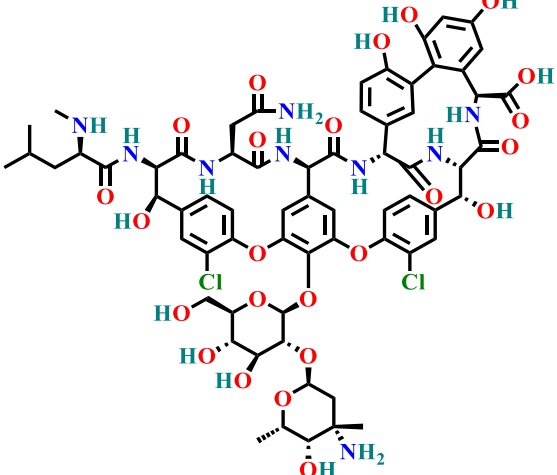
2.3. Molecular dynamic simulation

The MD simulations for the crystallized compound 1 and 2 were carried out against 1MWT and 1NU7, Schrodinger 2020-2 suite of Desmond modules was used to study the stability of the receptor-ligand system. The OPLS2005 force field had been used to simulate water molecules and evaluate the atomic interaction with the help of the predetermined TIP3P water model technique [28]. The shape and size of the repeating unit buffered at 10 \AA distances which were specified using cubic periodic boundary conditions. Sufficient Na^+ alongside salt atoms were added to balance the system charge and were randomly positioned in the sol-

Table 1
Crystal structure data and refinement details of compound 1 and 2.

Parameter	Compound 1	Compound 2
CCDC deposit No.	1938902	2075621
Empirical formula	C ₁₆ H ₁₆ OS	C ₁₂ H ₉ OS
Formula weight	256.36	215.27
Temperature (K)	293K	293K
Wavelength (Å)	0.71073 Å	0.71073
Crystal system, space group	Monoclinic, P21/n	Monoclinic, P21/n
Unit cell dimensions		
<i>a</i> (Å)	10.794(5)	12.060(4)
<i>b</i> (Å)	5.9290(18)	5.7311(15)
<i>c</i> (Å)	20.644(9)	15.336(6)
α (°)	90	90
β (°)	97.81(2)	98.080
γ (°)	90	90
Volume Å ³	1308.9(9)	1049.5(6)
<i>Z</i>	4	4
Density(calculated) in Mg m ⁻³	1.301	1.362
Absorption coefficient (mm ⁻¹)	0.232	0.277
<i>F</i> ₀₀₀	544	448
θ range for data collection	3.32° to 27.61°	3.41° to 27.52°
Index ranges	$-7 \leq h \leq 13$ $-7 \leq k \leq 7$ $-26 \leq l \leq 22$	$-13 \leq h \leq 15$ $-7 \leq k \leq 7$ $-19 \leq l \leq 10$
Reflections collected	4494	3805
Independent reflections	2793 [<i>R</i> _{int} = 0.0922]	2358 [<i>R</i> _{int} = 0.0922]
Refinement method	Full matrix least-squares on <i>F</i> ²	Full matrix least-squares on <i>F</i> ²
Data/restraints/parameters	2793 / 0 / 166	2358 / 0 / 136
Goodness-of-fit on <i>F</i> ²	0.975	1.068
Final [<i>I</i> > 2σ(<i>I</i>)]	<i>R</i> 1 = 0.0660, <i>wR</i> 2 = 0.1086	<i>R</i> 1 = 0.0647, <i>wR</i> 2 = 0.1364
<i>R</i> indices (all data)	<i>R</i> 1 = 0.1671, <i>wR</i> 2 = 0.1510	<i>R</i> 1 = 0.1018, <i>wR</i> 2 = 0.1600
Largest diff. peak and hole e Å ³	0.203 and −0.240	0.279 and −0.335

Table 2
Docking score of the compound 1, compound 2 and Vancomycin with 1NU7 and 1MWT proteins of MRSA.

Compound	Structure	Docking Score in kcal/mol	
		1NU7	1MWT
Compound 1		−6.0	−6.0
Compound 2		−7.1	−6.9
Vancomycin		−8.6	−8.3

vated system to nullify the system electrically. After building the solvated system containing the protein complex with the ligand, the compound was kept with a convergence threshold of 1 kcal mol⁻¹Å by using the conjugate gradient algorithm. The NPT ensemble was used to run molecular dynamics simulations with specific boundary conditions [29]. The temperature and pressure were maintained at 300 K throughout the process and subjected to a 20 ns run. Schrodinger's maestro interface 2020-2 was used to make all of the molecular dynamic simulation snapshots [30,31].

2.4. ADME and toxicity prediction

The standard pharmacokinetics (absorption, distribution, metabolism and excretion) and drug-likeness were determined for the estimation of the drug-likeness and pharmacokinetics parameters in the field of the drug discovery process [32]. Both the crystal structures were drawn on Marvin JS software in 2-D structure format and converted into SMILES using Swiss-ADME online tool (<http://swissadme.ch/>). The pkCSM online tool was used for the prediction of ADMET [33]. This includes Intestinal absorption, skin permeability, BBB permeability, CNS permeability, renal OCT2 substrate, AMES toxicity, oral rat acute toxicity, oral rat chronic toxicity and skin sensitization.

3. Results and discussions

3.1. Chemistry

The structure of the synthesized chalcone analogues were corroborated based on spectral techniques such as FT-IR, ¹H-NMR, and mass spectrometry. The structure and physical data of analogues are depicted in Table 2. Theoretically, values and experimentally determined values of elemental analysis lies within ± 0.4 %. The FT-IR spectra of synthesized two chalcones were recorded using KBr pellets in the range of 4000–400 cm⁻¹. There is a strong, broad absorption band that appeared at 1654 and 1647 cm⁻¹ were assigned to the C=O. The absorption bands at 1588 & 1592 cm⁻¹ are due to the presence of C=C stretch. The absorption band at 720 & 716 cm⁻¹ is due to the C-S stretch in synthesized compounds.

The ¹H NMR spectra for the synthesized chalcones were recorded using CDCl₃. Their peak multiplicity and integration assigned the expected resonances. The spectral integration shows good accordance with the synthesized chalcones. The ¹H NMR spectral data of aldehyde proton (-CHO) around δ 10.0 ppm is absent in the spectra of all synthesized compounds, which confirms the formation of α , β -unsaturated compounds (Chalcones). The proton spectral data following with respect to the number of protons and their chemical shifts with the proposed structures. The synthesized chalcones were further confirmed by the existence of a molecular ion peak in mass spectra. Mass spectra of the synthesized compounds showed an M⁺ fragmentation peak in agreement with their molecular formula. The mass spectra of compound 1 showed molecular ion peak at m/z 215.04 which is in accord with the molecular formula C₁₂H₉NOS, and mass spectra of compound 2 showed molecular ion peak at m/z 256.09 which is in accord with the molecular formula C₁₆H₁₆SO, Fig. 1 illustrates the mass spectra of compounds 1 and 2.

3.2. Crystal growth and XRD

Single crystals of both compound 1 and 2 were grown by a slow evaporation method using methanol solvent. Both compound 1 and 2 were crystallized in the monoclinic P 21/n space group, confirmed by the single crystal x-ray diffraction study. The molecular structure of compound 1 is significantly non-planar whereas

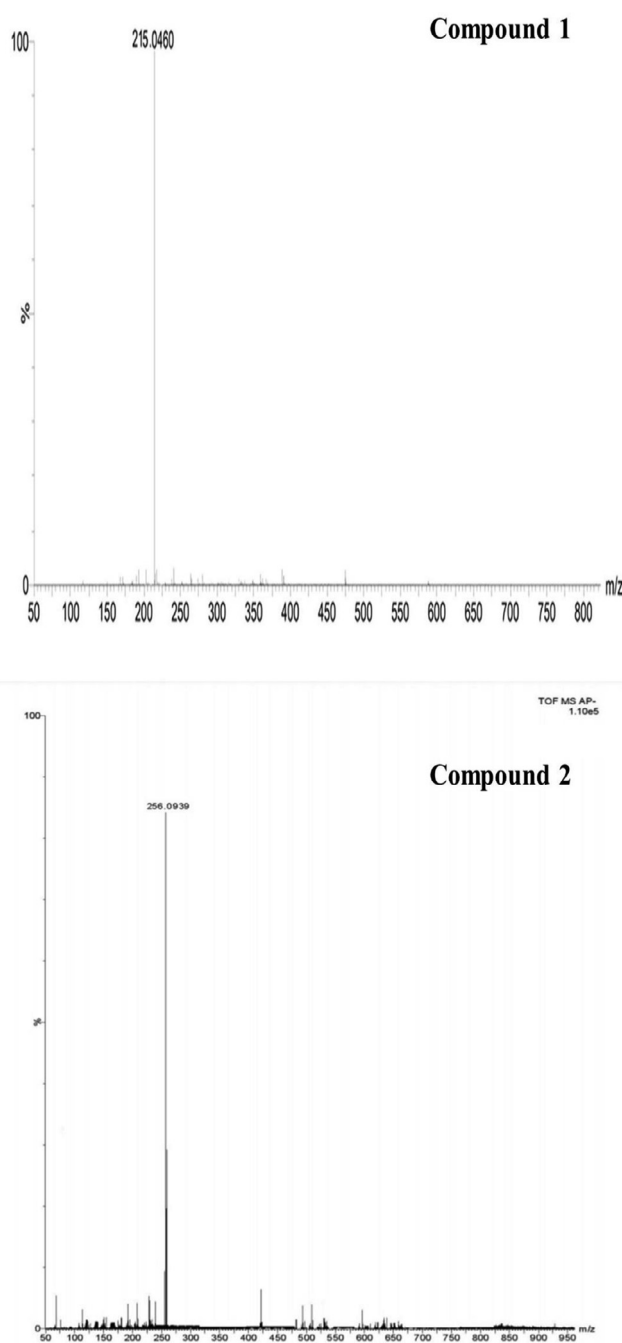


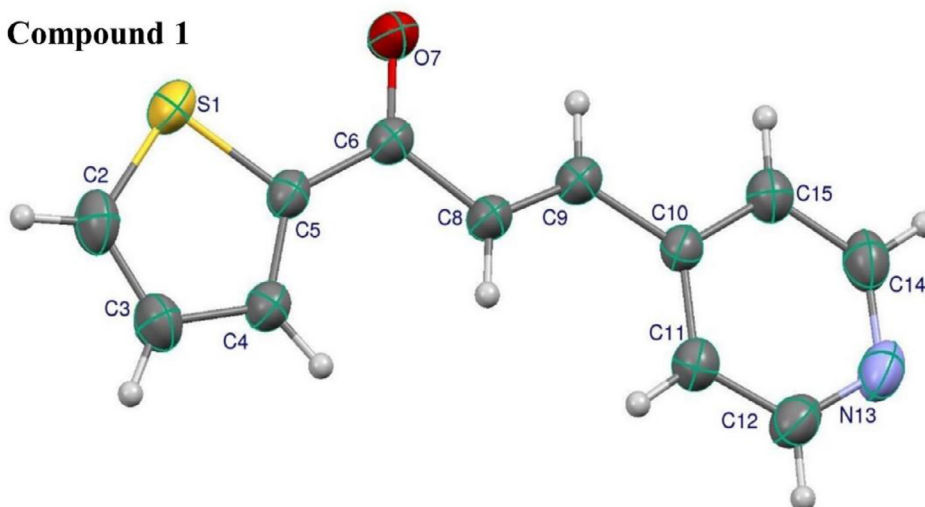
Fig. 1. Mass spectra of both compound 1 and 2.

compound 2 has coplanar structure. ORTEP of the molecule's compound 1 and 2 with thermal ellipsoids drawn at 50% probability are shown in Fig. 2. The crystallographic information of the molecules is given in Table 1. Bond lengths, bond angles, and torsional angles of both compound 1 and 2 are given in supplementary Tables S1 and S2.

The crystal structures of compound 1 and 2 are stabilized by various types of inter and intramolecular interactions.

Methyl group of compound 2 played a major role in stabilizing the crystal structure by forming intermolecular hydrogen bond interactions. C18 atom of compound 2 formed hydrogen bond interaction with the Oxygen atom of the adjacent molecule with the donor-acceptor distance of 2.63 Å and Hydrogen atoms of the methyl group interacted with the adjacent molecules to form two different short interactions with a distance of 2.33 Å. All these

Compound 1



Compound 2

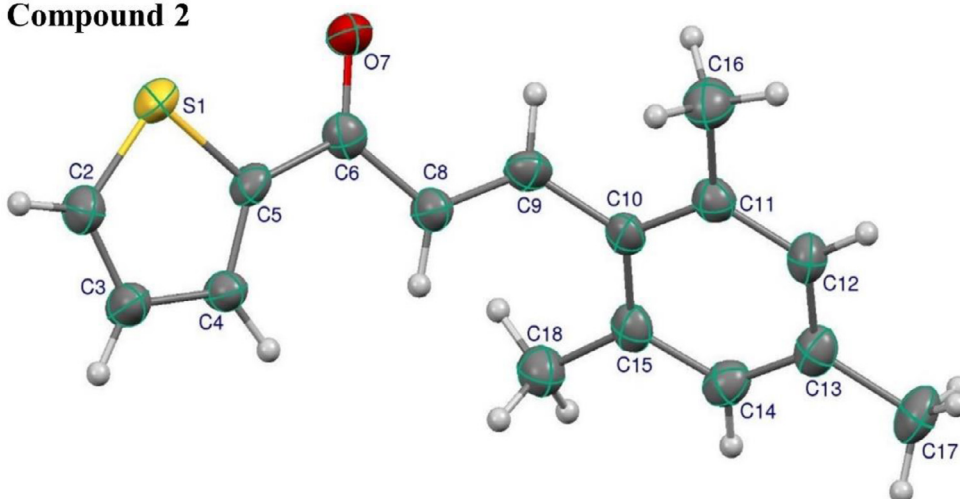


Fig. 2. ORTEP of compound 1 and 2 with thermal ellipsoids are drawn at 50% probability.

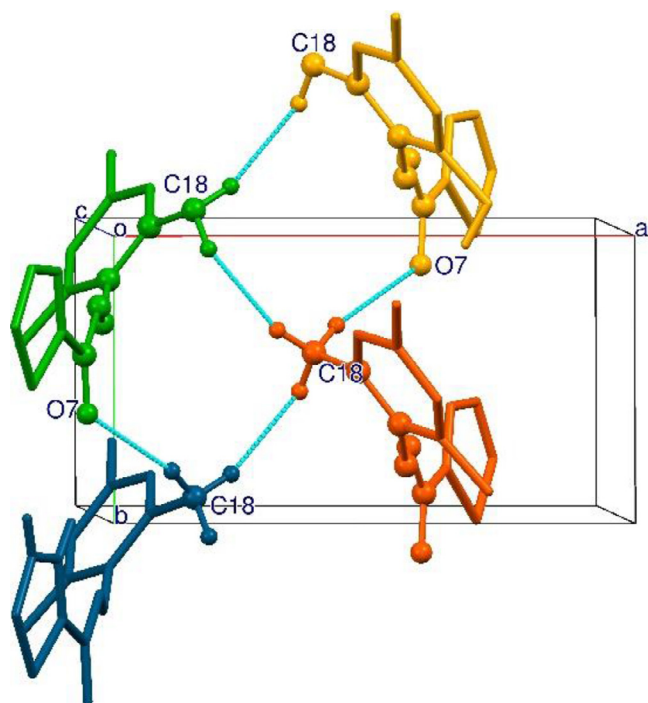


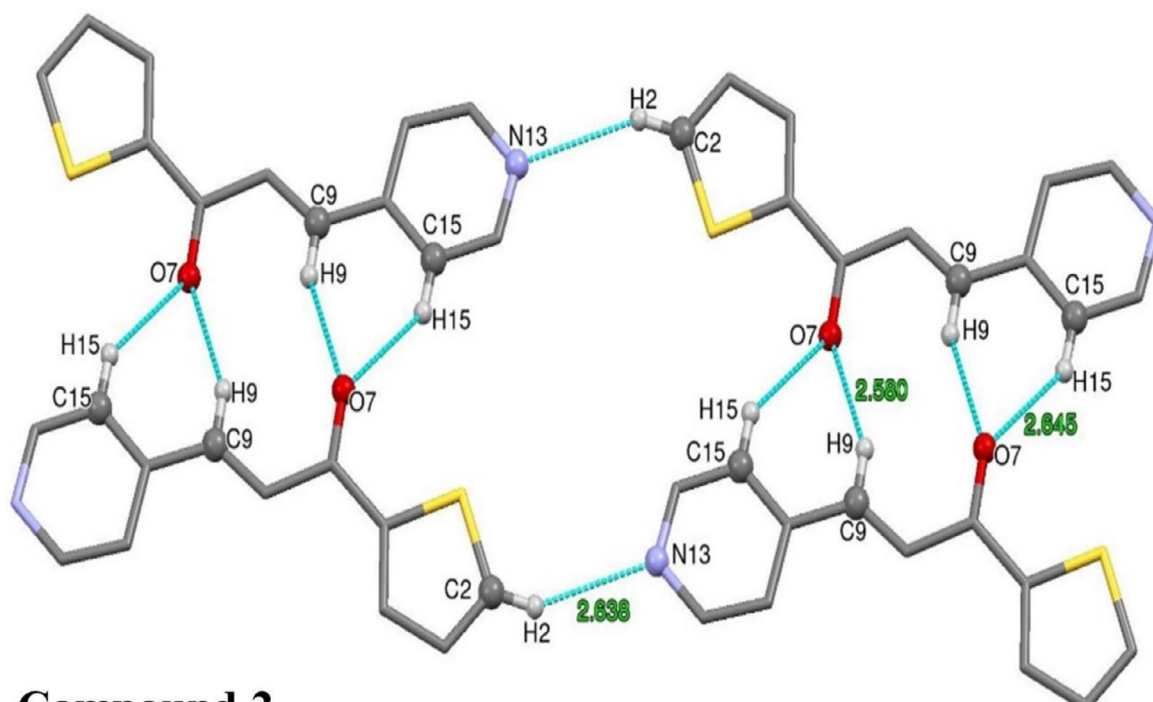
Fig. 3. Supramolecular synthon of compound 2 along crystallographic ab-plane.

three interactions of compound 2 combine to form a supramolecular synthon along the crystallographic ab-plane shown in Fig. 3.

C16-H16A...C13 (2.838 Å), C18-H18C...O7 (2.638 Å), C4-H4...O7 (2.658 Å), and C3-H3...S1 (2.915 Å) intermolecular interactions in compound 2 contributed to molecular stability by constructing three supramolecular $R_2^2(13)$, $R_2^1(11)$ and $R_2^2(8)$ ring motifs Fig. 4. C-H... π interaction between the methyl group and the centroid of thiophene ring with a distance of 2.98 Å and π ... π interaction between thiophene rings with a distance of 4.88 Å of the adjacent molecules are also played a key role in stabilizing the crystal structure of compound 2 shown in Fig. 5.

Crystal structure of compound 1 exhibits C-H...O intra and intermolecular hydrogen bond interactions, C-H... π , C-O... π and π ... π interactions greatly contribute to the formation of crystal packing and molecular stability of compound 1. C9-H9...O7 intramolecular hydrogen bond interaction [D-H: 0.93 Å, H...A: 2.49 Å, D...A: 2.822(4) Å and D-H...A: 101°] form the S(5) ring motif whereas, C9-H9...O7 intermolecular hydrogen bond interaction [D-H: 0.93 Å, H...A: 2.58 Å, D...A: 2.3.392(4) Å, D-H...A: 146° and symmetry code: 1-x, 2-y, -z] lead to the formation of $R_2^2(10)$ supramolecular ring motif. These two intra and intermolecular hydrogen bond interactions combined to form four membered $R_2^2(4)$ parallelogram ring motifs along crystallographic axes (Fig. 6). C2-H2...N13 and C15-H15...O7 interactions joined to construct a supramolecular $R_4^4(20)$ synthon along b-axis (Fig. 4). C12-H12...Cg2 intermolecular interactions contributed to the crystal structure packing of compound 1

Compound 1



Compound 2

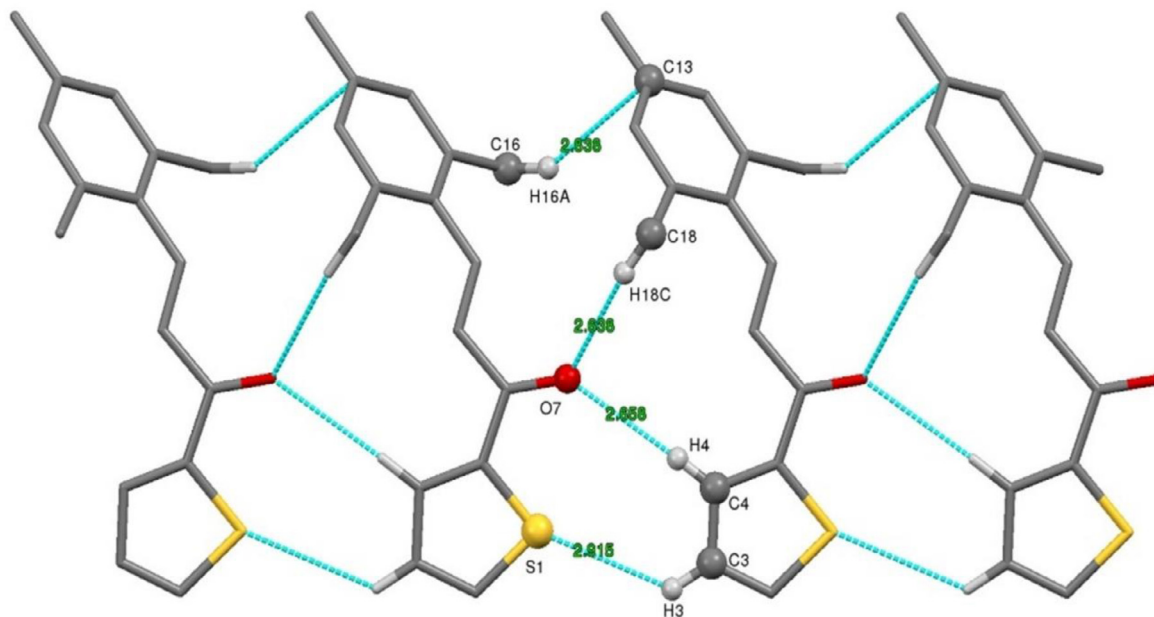


Fig. 4. Various supramolecular ring motifs of compound 1 and 2 formed by intermolecular hydrogen bond interactions.

with the H...Cg and O...Cg distance of 2.91 and 3.687(3) Å, respectively, where Cg2 is the centroid of the pyridine ring (Fig. 7).

3.3. Molecular docking

The molecular docking study of synthesized compounds with MRSA proteins (PDB ID 1NU7 & 1MWT) was investigated. *Staphylococci* coagulase-positive from *S. aureus* is a very well-known pathogen that can cause several infections. Coagulase triggers the

central coagulation zymogen, prothrombin, conformationally during host infection, thereby activating the cleavage of fibrinogen to fibrin. This model explains the coagulant properties and efficient fibrinogen by coagulase enzyme [34]. *S. aureus*, susceptible to β -lactam antibiotics owing to the irreversible acylation of the active site serine by the β -lactam antibiotics, the transpeptidase function of PBP2a is lost. PBP2a inhibition leads to abnormalities such as elongation, lesions, loss of selective permeability, and subsequent cell death and lysis in the structure of the cell wall. Also, MRSA be-

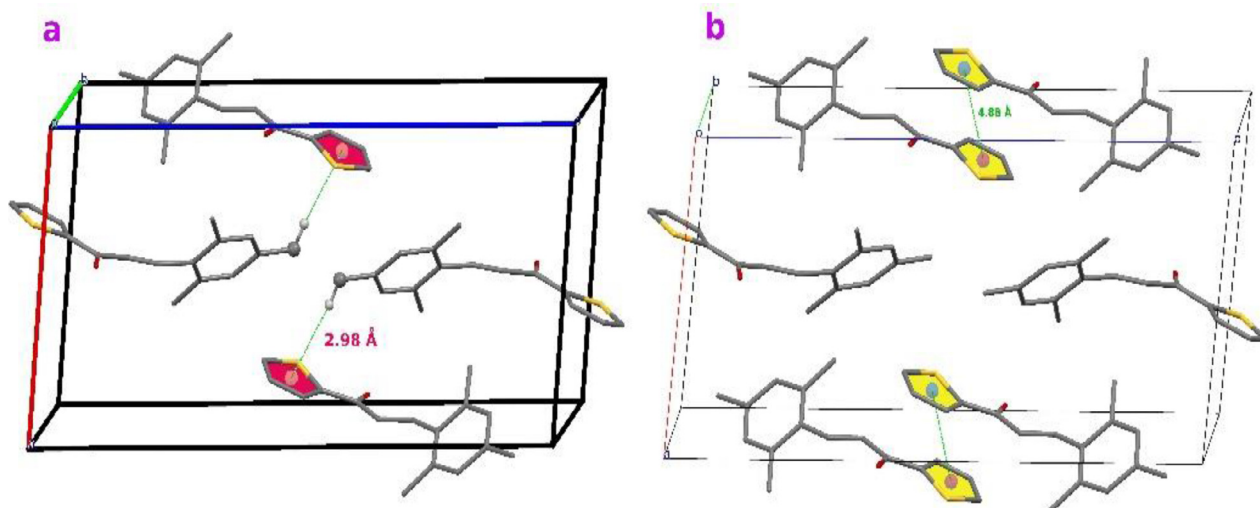


Fig. 5. C-H... π interaction between methyl group and the centroid of thiophene ring (a) and π ... π interaction between thiophene rings (b) of compound 2.

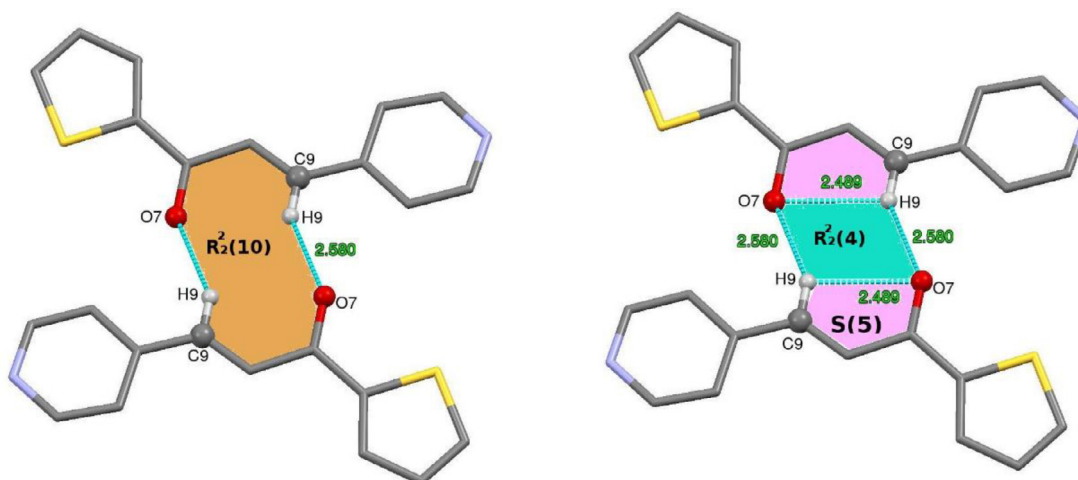


Fig. 6. Intra and intermolecular hydrogen bond interactions of compound 1 leads to formation of different graph set descriptors.

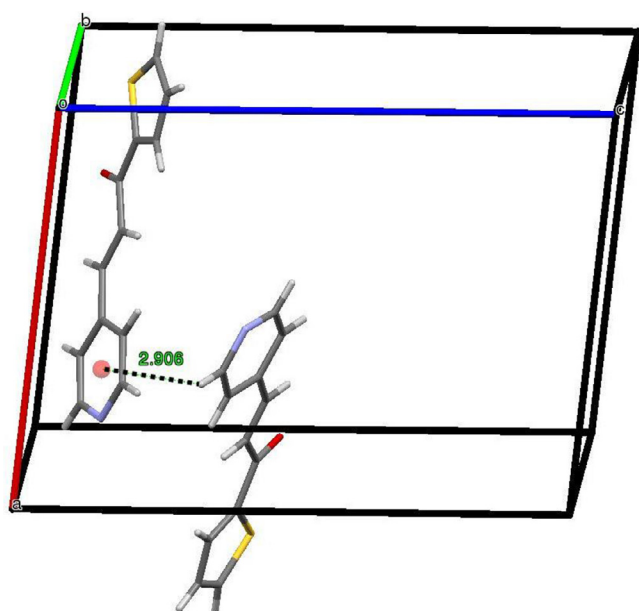


Fig. 7. C-H... π Intermolecular interactions contributed to the crystal structure packing of compound 1.

comes immune to β -lactam acylation due to the presence of PBP2a and successfully catalyzes the DD-transpeptidation reaction, which is essential to accomplish cell wall formation. PBP2a is therefore considered a prime candidate for inhibition of MRSA. To analyze the difference in binding efficiency of compound 1 and 2 against the allosteric site of PBP2a, molecular docking analysis was carried out.

The binding component of the compound was found to be present in the active binding sites. Compound 1 binds to protein residues of LYS145, THR147, GLY219, CYS191, GLU217 and so on of 1NU7 protein, the close contact of pyridine ring with THR147 amino acid residue with distance 2.09 Å through hydrogen bond interaction, and oxygen of carbonyl group make interaction through hydrogen bonding with GLY219 with distance 2.59 Å was observed in compound 1, and HIS583, SER403, ASN464, GLU294, TYR272, LYS273 and so on of allosteric site of the 1MWT protein with varying forms of interaction. Oxygen of carbonyl group make interaction through hydrogen bonding with LYS273 with distance 2.13 Å was observed in compound 1. The compound 1 showed a docking score of -6.0 kcal/mol with 1NU7 coagulase protein and -6.3 kcal/mol and -6.0 kcal/mol with 1MWT allosteric site of the protein. Compound 2 is found to exhibit the docking score of -7.1 kcal/mol with 1NU7 coagulase protein and a score of -6.9 kcal/mol at the active and allosteric site of the 1MWT protein.

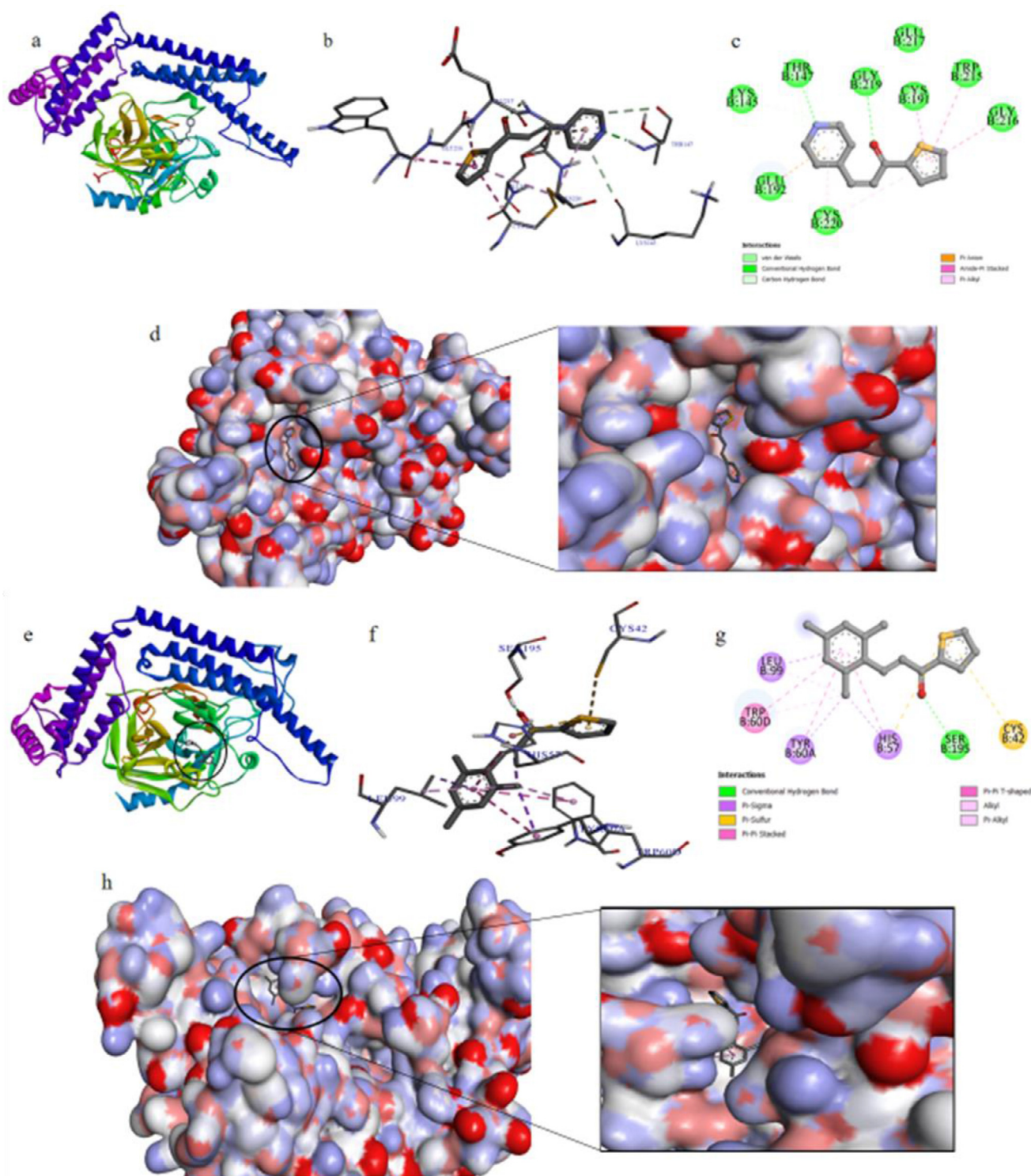


Fig. 8. Protein ligand complex of compound 1 with active site of 1NU7 (a & b), molecular docking 2D interaction of compound 1 (c), and interaction inside the binding pocket (d). Protein ligand complex of compound 2 with active site of 1NU7 (e & f); molecular docking 2D interaction of compound 2 (g), and interaction inside the binding pocket of protein (h).

Compound 2 is found to exhibit interaction with various amino acids like LEU99, CYS42, HIS57, ALA642, SER462, VAL256, and so on of 1NU7 and an allosteric site of 1MWT protein. The docking interaction images of compound 1, compound 2, and Vancomycin are illustrated in Figs. 8–10. Here in our study compound 2 being the potent antibacterial agent against 1NU7 and 1MWT

proteins, displayed the score of -7.1 and -6.9 kcal/mol which is comparable to the standard drug vancomycin with the score of -8.6 and -8.3 kcal/mol, respectively. The docking scores for the tested compounds revealed that synthesized admixtures could interact with one or more amino acids in the receptor's binding pocket. The docking results and specific interactions (bond length

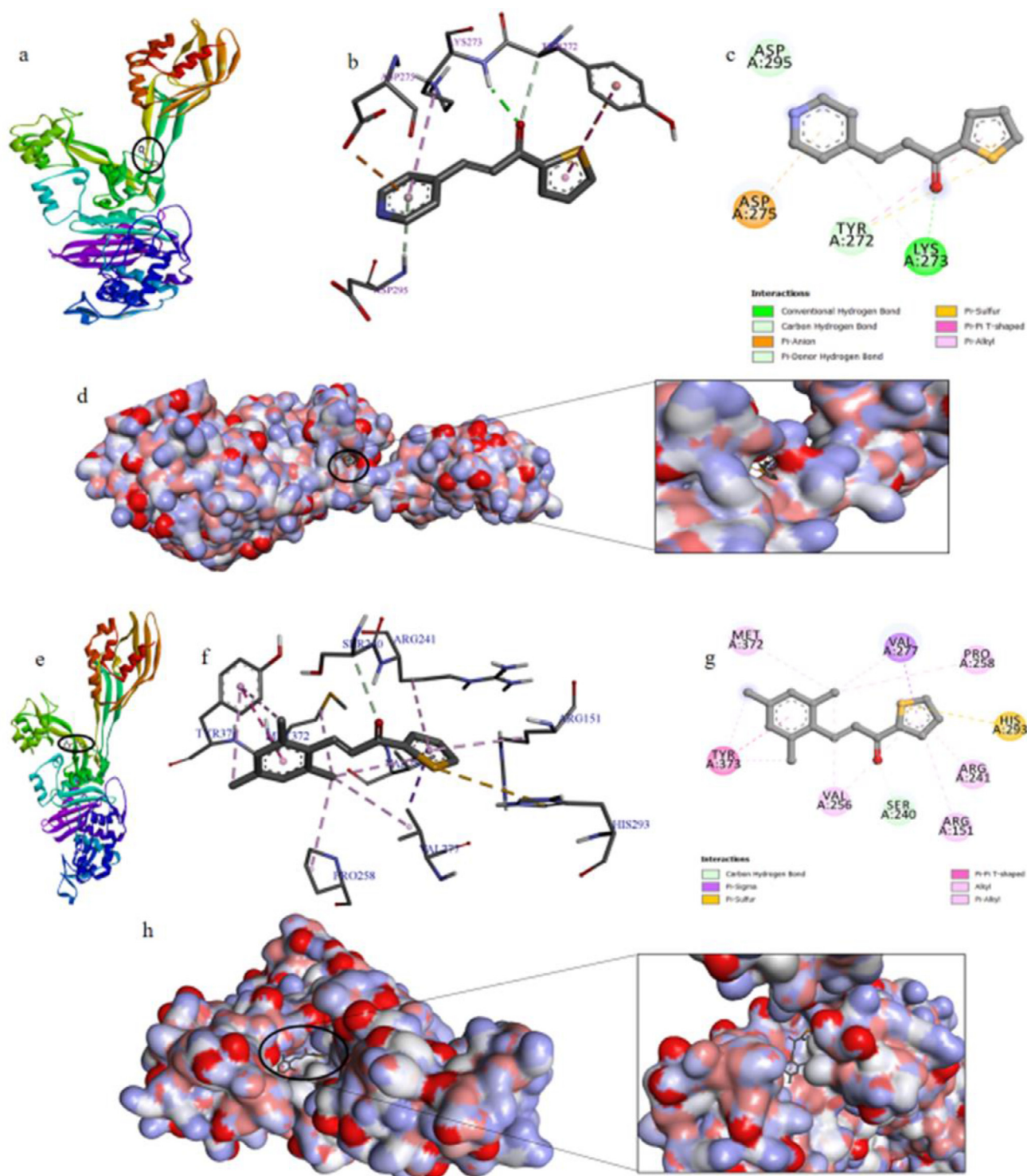


Fig. 9. Protein ligand complex of compound 1 with allosteric site of 1MWT (a & b), molecular docking 2D interaction of compound 1 (c), and interaction inside the binding pocket (d). Protein ligand complex of compound 2 with allosteric site of 1MWT (e & f), molecular docking 2D interaction of compound 2 (g), and interaction inside the binding pocket of protein (h).

and docking energies) in the binding phase are shown in Tables 2 and 3.

3.4. Molecular dynamic simulation

MD simulation was used to investigate confirmative stability, structural model alterations, internal movements, scoring and pre-

dicting stronger ligand-receptor interactions after docking studies, and so on [35]. In the present investigation the root mean square deviation (RMSD), the root mean square fluctuation (RMSF) analysis of various interactions, and percentage of hydrogen bond formation compound 1 & 2 with *Staphylocoagulase* (1NU7) and PBP2a (1MWT) proteins. According to docking interaction, RMSD revealed compound 1 with 1NU7 produced excellent interaction and dock-

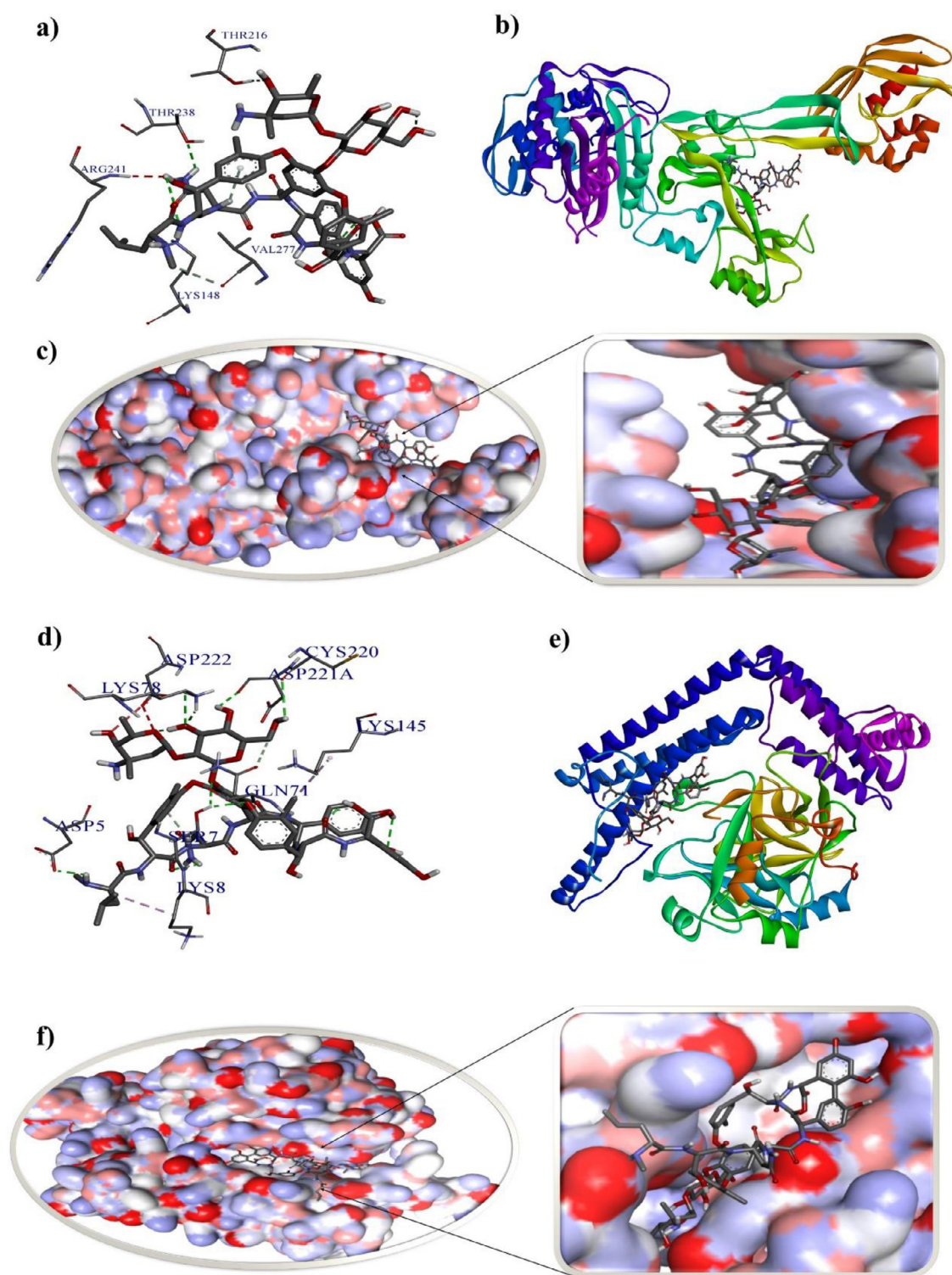


Fig. 10. Protein ligand complex of vancomycin with the allosteric site of 1MWT (a & b) and interaction inside the binding pocket (c). Protein ligand complex of vancomycin with active site of 1NU7 (d & e) and interaction inside the binding pocket of protein (f).

Table 3

Specific interaction of synthesized compound 1, 2 and Vancomycin with 1NU7 and 1MWT protein of MRSA.

Protein PDB ID	Compound	Residue involved	Ligand	Interaction type	Distance (Å)
1NU7	Compound 1	THR147	N of Pyridine	Hydrogen	2.09
		GLY219	O of Carbonyl group	Hydrogen	2.59
		THR147	group	Carbon	3.68
		LYS 145	C of Pyridine	Carbon	3.78
		CYS191	C of Pyridine	Amide π stacked	3.84
		GLU192	π of Thiophene	π Anion	4.29
		TRP215	π of Pyridine	Amide π stacked	4.61
	Compound 2	GLY216	π of Thiophene	Amide π stacked	4.99
		SER195	O of Carbonyl group	Hydrogen	2.36
		TYR60A	group	π sigma	3.63
		HIS57	CH ₃ group	π sigma	3.84
		LEU99	CH ₃ group	π sigma	3.91
		TRP60D	π of Benzene	π alkyl	4.12
		HIS57	CH ₃ group	π sulfur	4.72
	Vancomycin	LEU99	S of Thiophene	Alkyl	5.00
		LYS78	CH ₃ group	Hydrogen	2.13
		ASP5	Oxygen	Hydrogen	2.28
		SER7	Hydrogen	Hydrogen	2.47
		ASP221A	Oxygen	Hydrogen	2.53
		SER7	Hydrogen	Hydrogen	2.61
		LYS78	Oxygen	Hydrogen	2.70
		CYS220	Hydrogen	Hydrogen	3.04
		LYS8	Carbon	Alkyl	3.93
	Compound 1	LYS273	O of Carbonyl group	Hydrogen	2.13
		ASP295	group	π Donor	2.71
		TYR272	π of Pyridine	Carbon	3.11
		ASP275	O of Carbonyl group	π Anion	3.91
		TYR272	group	π sulfur	3.95
		LYS273	π of Pyridine	π alkyl	5.02
		S of Thiophene	π of Pyridine		
	Compound 2	SER240	O of Carbonyl group	Carbon	3.59
		VAL277	group	π sigma	3.70
		VAL277	π of Thiophene	Alkyl	4.67
		PRO258	CH ₃ group	Alkyl	4.74
		MET372	CH ₃ group	Alkyl	4.87
		VAL256	CH ₃ group	Alkyl	5.00
		HIS293	CH ₃ group	π sulfur	5.00
		TYR373	S of Thiophene	π - π T shaped	5.01
		ARG151	π of Benzene	π alkyl	5.03
		ARG241	π of Thiophene	π alkyl	5.06
		π of Thiophene			
	Vancomycin	LYS148	Oxygen	Hydrogen	1.93
		THR238	Hydrogen	Hydrogen	2.52
		LYS148	Oxygen	Hydrogen	2.64
		THR216	Oxygen	Hydrogen	2.67
		VAL277	Carbon	Alkyl	3.79

ing results with both *Staphylocoagulase* (1NU7) and PBP2a (1MWT) proteins. Compound 1 had a strong interaction up to 9 ns (0.7 Å to 3.2 Å) with 1NU7; this gradually decreased up to 20 ns, while compound 2 showed a moderate interaction up to 9 ns (0.6 Å to 3.8 Å), low interaction up to 10–17.5 ns (2.0 Å to 4.0 Å) and it showed a good interaction up to 17.5–20 ns (3.0 Å to 4.2 Å) with 1NU7 as shown in Fig. 11. The RMSF graph of compound 1 showed that the significant peaks of fluctuations have been observed initially, residue number 380 up to 4.8 Å, residues between 430 and 490 with up to 2.1 Å, residues number 550 up to 2.8 Å and residues number 290 up to 5 Å get the maximum deviation. While RMSF graph of compound 2 showed that residues number 310 up to 4.0 Å, residues number 550 up to 4.8 Å, residue number 290 and 380 up to 6.4 Å get the maximum deviation throughout the MD simulations. The remaining residues were known to be moderately stable and fluctuating well below 2.0 Å. Compound 1 had

an H-bonding interaction of up to 0.04 with 1NU7's ARG221 and SER195 amino acids, while compound 2 had an H-bonding interaction of up to 0.03 with TRP60 and LYS60 amino acids. Water bridge bonding and hydrophobic bonds were visible in the remaining areas. Frequent direct H-bonds of compound 1 were observed with residues GLU192, GLU146, and HIS57, respectively. Similarly, compound 2 had 61% interaction with the HIS57. However, both the results were found to be converging after 20 ns of simulated time it can be concluded that compound 2 had greater interaction stability with active amino acids of 1NU7 than compound 1. Fig. 11 and 12 reveal RMSD, RMSF, protein-ligand contacts, and ligand-protein contacts of compound 1 and 2 with 1NU7 and 1MWT protein, respectively.

RMSD of compound 1 with 1MWT protein had a low interaction up to 10 ns (1.9 Å to 5.4 Å) with 1MWT and subsequently showed a good interaction up to 20 ns, while compound 2 showed

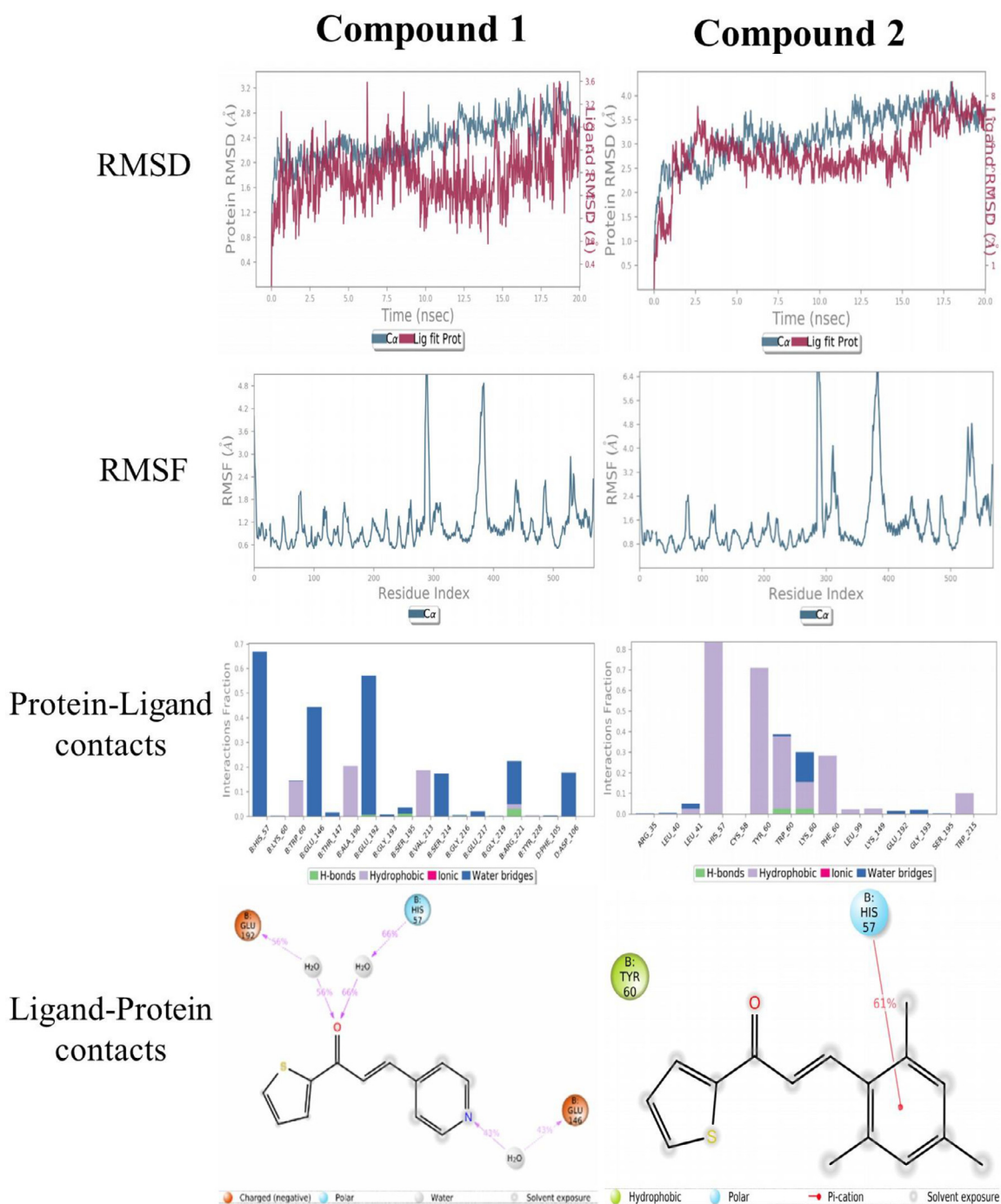


Fig. 11. Illustration to show the outcomes of molecular dynamic simulation of Compound 1 and 2 complexes. RMSD, RMSF of the backbone over the 20 ns MDS at 300 K of the complexes systems. Protein (1NU7) ligand interaction (P-L contacts) & 2D- Diagram of Ligand Protein (L-P Contacts) interaction.

a moderate interaction up to 20 ns (1.6 Å to 6.4 Å) with the 1MWT. The significant peaks of compound 1 are fluctuated have been observed from the RMSF graph, initially, residue number 10–50 over 4.2 Å, residues number 60 and 180 up to 4.7 Å, residues number 360 up to 3.7 Å, and residues number 290 up to 4.9 Å get the maximum deviation. While RMSF graph of compound 2 showed that residues number 70 and 90 up to 5.1 Å, residues number 280 up to 6 Å, residue number 200 and 240 up to 4.1 Å, and residues number 180 up to 7 Å, get the maximum deviation throughout the

MD simulations. The remaining residues were known to be moderately stable and fluctuating well below 2.0 Å. Compound 1 had an H-bonding interaction of up to 0.04 with SER643 and ALA642 amino acids, while compound 2 had an H-bonding interaction of up to 0.08 with SER403, LYS597, and SER598 amino acids. Water bridge bonding and hydrophobic bonds were visible in the remaining areas. Frequent direct H-bonds of compound 1 were observed with residues ALA146, and HIS57, respectively. Similarly, compound 2 had 81% and 47% interaction with the HIS583 along with 31% in-

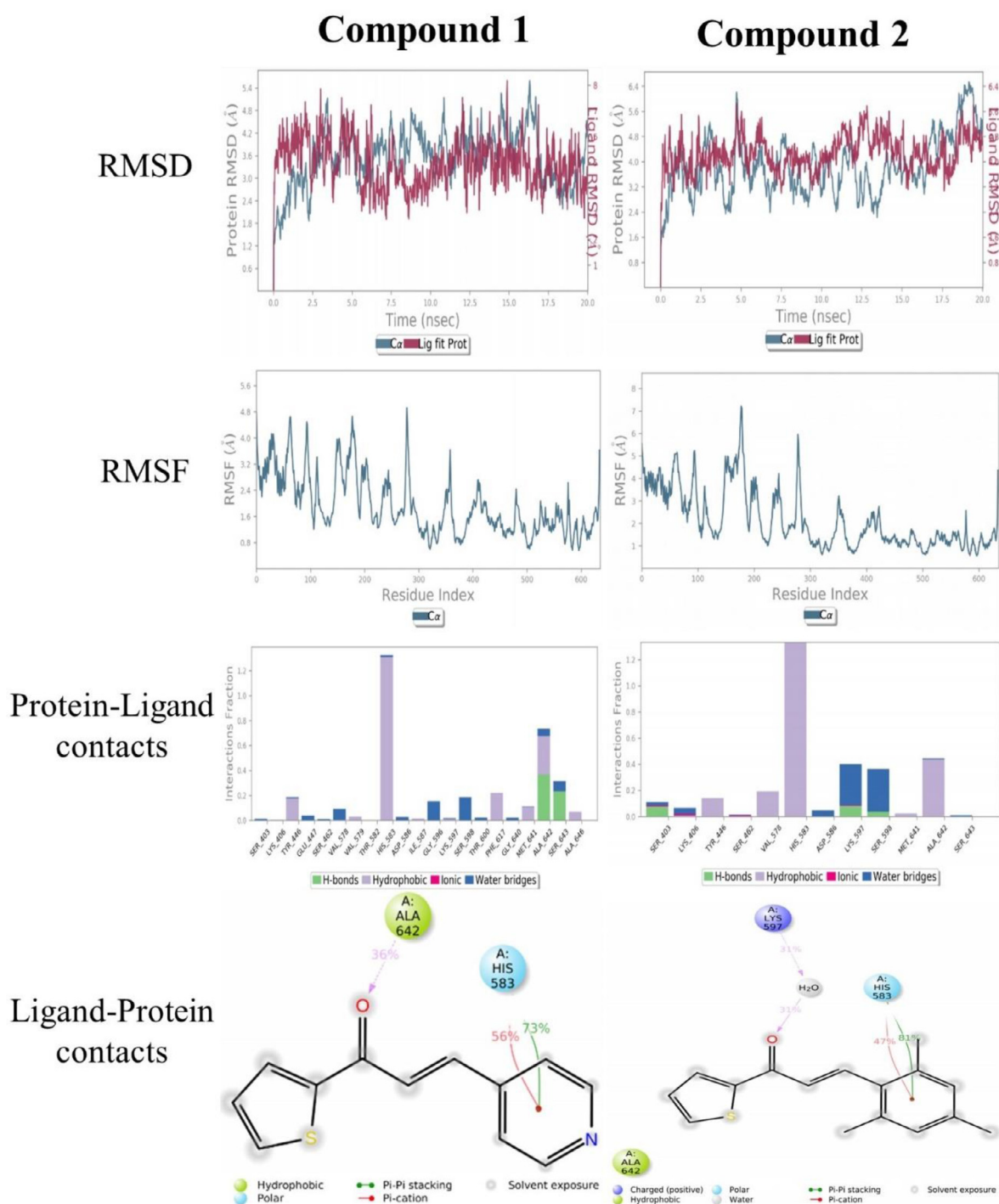


Fig. 12. Illustration to show the outcomes of Molecular dynamic simulation of Compound 1 and 2 complexes. RMSD, RMSF of the backbone over the 20 ns MDS at 300 k of the complexes systems. Protein (1MWT) ligand interaction (P-L contacts) & 2D- Diagram of Ligand Protein (L-P Contacts) interaction.

teraction with LYS597. Hence it can be concluded that compound 2 had greater interaction stability with amino acids of 1MWT than compound 1.

3.5. ADMET and toxicity predictions

ADMET properties were predicted to evaluate potential lead candidate. Toxicity prediction is one of the important methods of

the drug discovery and development process which consumes less time. The ADMET results of both compounds have been interpreted using pkCSM tool. The compounds show excellent gastrointestinal absorption and also a low skin permeability ($\log K_p > -2.5$). The compound exhibit properties such as P-glycoprotein substrate inhibitor (I and II), cytochrome P450 enzyme inhibitor are shown in Table 4. Compound 2 reveals a high value of $\log VD_{ss}$. Both the compounds are readily cross the blood brain-barrier and penetrate

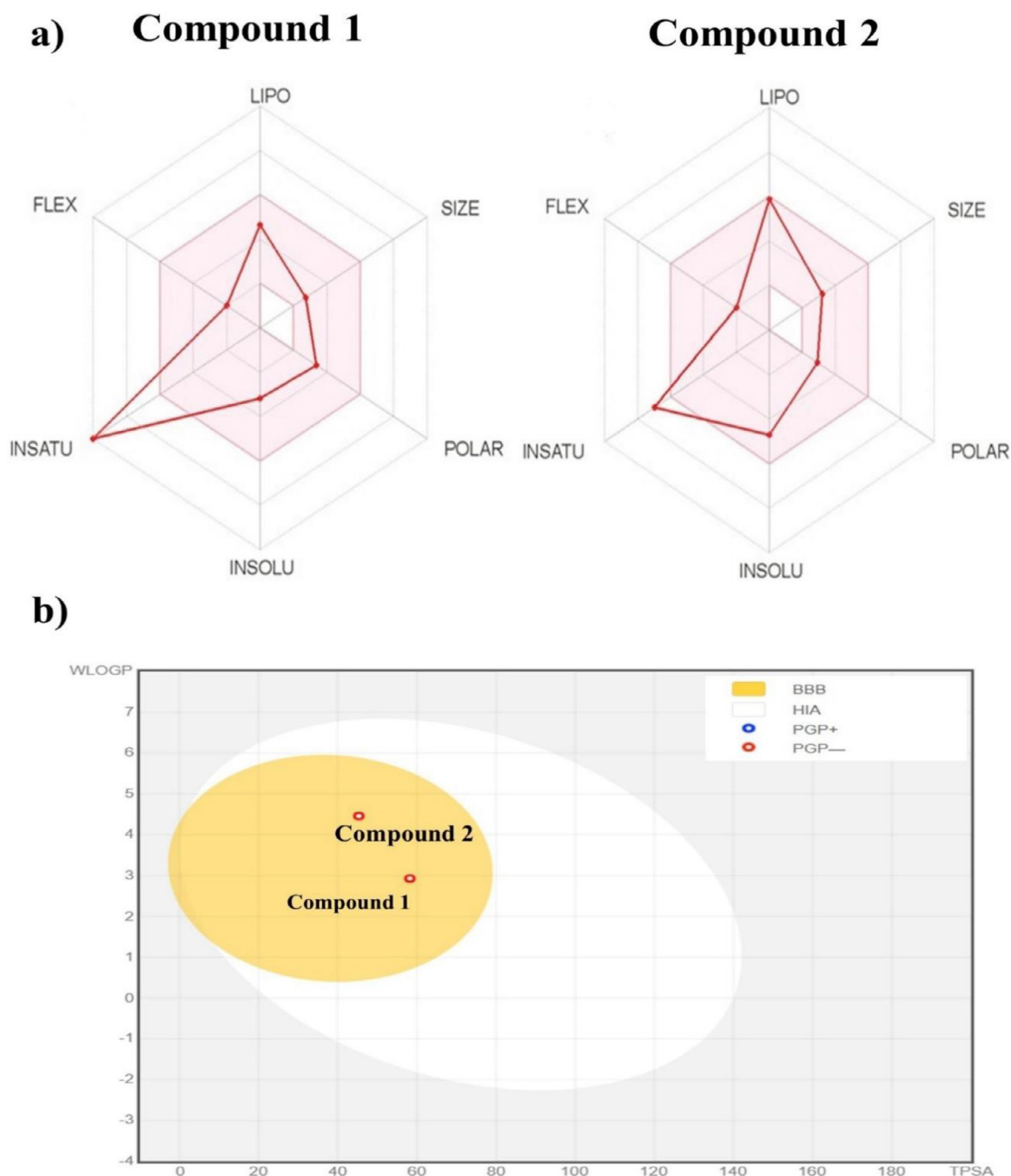


Fig. 13. (a) Bioavailability radar and (b) Boiled-Egg image of compound 1 and 2.

the central nervous system. Both compounds are not likely to be renal OCT2 substrates. Both compounds are not showing an AMES toxic nature and also compounds reveal a high maximum tolerated dose for human. The oral rat acute and chronic toxicity were also studied and results have been interpreted. Hepatotoxicity and skin sensitization of both compounds were studied and results are shown in Table 4. In Minnow toxicity compound 2 is regarded as high acute toxicity. Both compounds obey all the 5 rules of drug-likeness including Lipinski, Ghose, Veber, Egan, and Muegge rules

and the results were depicted in Table 5. Boiled-egg model of compounds 1 and 2 are shown in Fig. 13.

ADMET study of vancomycin revealed that it has poor gastrointestinal absorption and low skin permeability ($\log K_p > -2.5$), low value of $\log VD_{ss}$ ($\log VD_{ss} < -0.15$), inhibitors of cytochrome P450 enzyme, vancomycin, does not obey all the five rules of drug-likeness including Lipinski, Ghose, Veber, Egan and Muegge rules. ADMET results of vancomycin was depicted in supplementary Tables S3 and S4 and boiled-egg model of vancomycin shown in Fig. S1.

Table 4
ADME and Toxicity by using pkCSM tool.

Parameters	Compound 1	Compound 2
Absorption	Water solubility (log mol/L)	-2.79
	Caco2 permeability (log Papp in 10 ⁻⁶ cm/s)	1.882
	Intestinal absorption (human) (% Absorbed)	96.27
	Skin Permeability (log Kp)	-1.872
	P-glycoprotein substrate	No
	P-glycoprotein I inhibitor	No
Distribution	P-glycoprotein II inhibitor	No
	VDss (human) (log L/kg)	-0.026
	Fraction unbound (human) (Fu)	0.187
	BBB permeability (log BB)	0.096
	CNS permeability (log PS)	-1.639
Metabolism	CYP2D6 substrate	No
	CYP3A4 substrate	No
	CYP1A2 inhibitor	Yes
	CYP2C19 inhibitor	Yes
	CYP2C9 inhibitor	Yes
	CYP2D6 inhibitor	No
	CYP3A4 inhibitor	No
	Total Clearance (log ml/min/kg)	0.015
Excretion	Renal OCT2 substrate	No
	AMES toxicity	No
Toxicity	Max. tolerated dose (human) (log mg/kg/day)	0.529
	hERG I inhibitor	No
	hERG II inhibitor	No
	Oral Rat Acute Toxicity (LD50) (mol/kg)	2.1
	Oral Rat Chronic Toxicity (LOAEL) (log mg/kg_bw/day)	2.104
	Hepatotoxicity	No
	Skin Sensitization	Yes
	<i>T. Pyriformis</i> toxicity (log ug/L)	1.343
	Minnow toxicity (log mM)	0.46
		-0.743

Table 5
Druglikeness by using Swiss-ADME tool.

Drug likeness	Compound 1	Compound 2
Lipinski	Yes	Yes
Ghose	Yes	Yes
Veber	Yes	Yes
Egan	Yes	Yes
Muegge	Yes	Yes
Violations	0	0

4. Conclusion

In the present investigation, new thiophene chalcones were synthesized and characterized by ¹H-NMR and IR spectroscopic techniques. The single crystal structures of thiophene chalcones were elucidated by X-ray diffraction study. In the crystal structure of 3-(3-pyridine-4-yl)-1-(thiophen-2-yl)prop-2-en-1-one and 3-mesityl-1-(thiophen-2-yl)prop-2-en-1-one, the molecules are connected via C-H...O and C3-H3...S1 hydrogen bonds which are greatly contributed to molecular stability. Molecular docking and molecular dynamics simulation studies revealed the interaction mode, binding energy, existence of hydrogen bonds, hydrophobic interactions and stability of protein-ligand complexes upto 20 ns simulation run. From the present investigation compound 2 showed a promising antibacterial activity against MRSA which can be develop as an antibacterial agent in futuristic studies.

Credit Author Statement

S. Nanjundaswamy: Methodology, Software, Writing-original draft, review and editing. **Gurumallappa:** Methodology, Software, **M. K Hema:** Software, Data curation, Writing-original draft. **C.S. Karthik:** Conceptualization, Writing - original draft, review and editing. **Muthu K. Gnanamani:** Writing - review and editing. **R.**

Jothi Ramalingam: Writing - review and editing. **N. K. Lokanath:** Writing - review and editing. **P Mallu:** Supervision, Writing - review and editing.

Declaration of Competing Interest

The authors declare that they have no known competing financial interests or personal relationships that could have appeared to influence the work reported in this paper.

Acknowledgment

The authors are thankful to SJCE, JSS Science and Technology University for providing supercomputing facility and VGST-CISEE Project (GRD 647), GOK, Karnataka, The author (R. J) express thankful and financial support by the Researchers Supporting Project Number (RSP-2021/354) King Saud University, Riyadh, Saudi Arabia.

Supplementary materials

Supplementary material associated with this article can be found, in the online version, at doi:[10.1016/j.molstruc.2021.131365](https://doi.org/10.1016/j.molstruc.2021.131365).

References

- [1] G.E. Delgado, J.A. Henao, J.H. Quintana, H.M. Al-Maqtari, J. Jamal, H.M. Sirat, Structural characterization of a new chalcone compound containing a thiophene moiety: (E)-3-(5-bromothiophen-2-yl)-1-(2, 5-dichlorothiophen-3-yl)-2-propen-1-one, *J. Struct. Chem.* 59 (6) (2018) 1440–1445.
- [2] R. Mishra, I. Tomer, S. Kumar, Synthesis and antimicrobial evaluation of novel thiophene derivatives, *Der Pharm. Sin.* 3 (2012) 332–336.
- [3] V.S. Naik, P.S. Patil, Q.A. Wong, C.K. Quah, N.B. Gummagol, H.S. Jayanna, Molecular structure, linear optical, second and third-order nonlinear optical properties of two non-centrosymmetric thiophene-chalcone derivatives, *J. Mol. Struct.* 1222 (2020) 128901.
- [4] C. Winter, J.N. Caetano, A.B.C. Araújo, A.R. Chaves, I.C. Ostroski, B.G. Vaz, C.N. Pérez, C.G. Alonso, Activated carbons for chalcone production: Claisen-Schmidt condensation reaction, *Chem. Eng. J.* 303 (2016) 604–610.
- [5] N.M. Rateb, H.F. Zohdi, Atom-efficient, solvent-free, green synthesis of chalcones by grinding, *Synth. Comm.* 39 (15) (2009) 2789–2794.

- [6] S. Eddarir, N. Cotelte, Y. Bakkour, C. Rolando, An efficient synthesis of chalcones based on the Suzuki reaction, *Tetrahedron Lett.* 44 (28) (2003) 5359–5363.
- [7] M.R. Ahmad, V.G. Sastry, N. Bano, S. Anwar, Synthesis of novel chalcone derivatives by conventional and microwave irradiation methods and their pharmacological activities, *Arab. J. Chem.* 9 (2016) S931–S935.
- [8] P.J. Sloomackers, A. Rasschaert, W. Janssens, J. Verhulst, The Friedel-Crafts acylation reaction. III. The Friedel-Crafts chalcone synthesis from substituted trans-cinnamoyl chlorides and toluene, *Bull. Soc. Chim. Belges* 75 (7–8) (1966) 433–448.
- [9] T. Guo, R. Xia, M. Chen, J. He, S. Su, L. Liu, X. Li, W. Xue, Biological activity evaluation and action mechanism of chalcone derivatives containing thiophene sulfonate, *RSC Adv.* 9 (43) (2019) 24942–24950.
- [10] B.P. Bandgar, S.A. Patil, R.N. Gacche, B.L. Korbadi, B.S. Hote, S.N. Kinkar, S.S. Jalde, Synthesis and biological evaluation of nitrogen-containing chalcones as possible anti-inflammatory and antioxidant agents, *Bioorg. Med. Chem. Lett.* 20 (2) (2010) 730–733.
- [11] E.J. Henry, S.J. Bird, P. Gowland, M. Collins, J.P. Cassella, Ferrocenyl chalcone derivatives as possible antimicrobial agents, *J. Antibiot.* 73 (5) (2020) 299–308 (Tokyo).
- [12] D.K. Mahapatra, S.K. Bharti, V. Asati, Chalcone derivatives: anti-inflammatory potential and molecular targets perspectives, *Curr. Top. Med. Chem.* 17 (28) (2017) 3146–3169.
- [13] C. Karthikeyan, N.S.H.N. Narayana Moorthy, S. Ramasamy, U. Vanam, E. Manivannan, D. Karunakaran, P. Trivedi, Advances in chalcones with anticancer activities, *Recent Pat. Anti cancer Drug Discov.* 10 (1) (2015) 97–115.
- [14] C.L. Miranda, J.F. Stevens, V. Ivanov, M. McCall, B. Frei, M.L. Deinzer, D.R. Buhler, Antioxidant and prooxidant actions of prenylated and nonprenylated chalcones and flavanones *in vitro*, *J. Agric. Food Chem.* 48 (9) (2000) 3876–3884.
- [15] N. Panigrahi, S. Ganguly, J. Panda, Synthesis, antimicrobial evaluation and molecular docking studies of novel oxazolidinone-thiophene chalcone hybrid derivatives, *Res. J. Pharm. Technol.* 11 (12) (2018) 5611–5622.
- [16] A.M. Asiri, S.A. Khan, Synthesis and anti-bacterial activities of a bis-chalcone derived from thiophene and its bis-cyclized products, *Molecules* 16 (1) (2011) 523–531.
- [17] L.S. Ming, J. Jamalis, H.M. Al-Maqtari, M.M. Rosli, M. Sankaranarayanan, S. Chander, H.K. Fun, Synthesis, characterization, antifungal activities and crystal structure of thiophene-based heterocyclic chalcones, *Chem. Data Collect.* 9 (2017) 104–113.
- [18] M.G. Prabhudeva, S. Bharath, A.D. Kumar, S. Naveen, N.K. Lokanath, B.N. Mylarappa, K.A. Kumar, Design and environmentally benign synthesis of novel thiophene appended pyrazole analogues as anti-inflammatory and radical scavenging agents: crystallographic, *in silico* modeling, docking and SAR characterization, *Bioorg. Chem.* 73 (2017) 109–120.
- [19] K. Mustikasari, J.E. Harap, T.B. Susilo, N. Komari, Molecular docking studies of indolyl-benzodioxyl-chalcone, pyrrolyl-benzodioxyl-chalcone, and thiophenyl-benzodioxyl-chalcone as an antimalarial agent, in: *Key Eng. Mater.*, 874, 2021, pp. 136–142. Trans Tech Publications Ltd..
- [20] C. Shruthi, V. Ravindrachary, B. Guruswamy, D.J. Prasad, J. Goveas, K. Kumara, N.K. Lokanath, Molecular structure, Hirshfeld surface and density functional theoretical analysis of a NLO active chalcone derivative single crystal—a quantum chemical approach, *J. Mol. Struct.* 1228 (2021) 129739.
- [21] C.C.S. Rigaku, Expert 2.0 r15. Software for Data Collection and Processing, Rigaku Corporation, Tokyo, Japan, 2011.
- [22] G.M. Sheldrick, Phase annealing in SHELX-90: direct methods for larger structures, *Acta Crystallogr. A* 46 (6) (1990) 467–473.
- [23] G.M. Sheldrick, Crystal structure refinement with SHELXL, *Acta Crystallogr. C* 71 (1) (2015) 3–8.
- [24] O.V. Dolomanov, L.J. Bourhis, R.J. Gildea, J.A. Howard, H. Puschmann, OLEX2: a complete structure solution, refinement and analysis program, *J. Appl. Crystallogr.* 42 (2) (2009) 339–341.
- [25] A.L. Spek, PLATON, an integrated tool for the analysis of the results of a single crystal structure determination, *Acta Crystallogr. A* 46 (s1) (1990) c34 c34.
- [26] C.F. Macrae, I. Sovago, S.J. Cottrell, P.T. Galek, P. McCabe, E. Pidcock, P.A. Wood, Mercury 4.0: from visualization to analysis, design and prediction, *J. Appl. Crystallogr.* (2020) 226–235.
- [27] N. Mani, S. Vijayakumar, L. PTV, A. Arunachalam, Allosteric site-mediated active site inhibition of PBP2a using Quercetin 3-O-rutinoside and its combination, *J. Biomol. Struct. Dyn.* 34 (8) (2016) 1778–1796.
- [28] S.V.G. Reddy, K.T. Reddy, V.V. Kumari, S.H. Basha, Molecular docking and dynamic simulation studies evidenced plausible immunotherapeutic anticancer property by Withaferin A targeting indoleamine 2, 3-dioxygenase, *J. Biomol. Struct. Dyn.* 33 (12) (2015) 2695–2709.
- [29] C.R. Sahoo, S.K. Paidesetty, B. Dehury, R.N. Padhy, Molecular dynamics and computational study of Mannich-based coumarin derivatives: potent tyrosine kinase inhibitor, *J. Biomol. Struct. Dyn.* 38 (18) (2020) 5419–5428.
- [30] W.L. Jorgensen, J. Chandrasekhar, J.D. Madura, R.W. Impey, M.L. Klein, Comparison of simple potential functions for simulating liquid water, *J. Chem. Phys.* 79 (2) (1983) 926–935.
- [31] W. Shinoda, M. Mikami, Rigid-body dynamics in the isothermal-isobaric ensemble: a test on the accuracy and computational efficiency, *J. Comput. Chem.* 24 (8) (2003) 920–930.
- [32] Z. Basharat, M. Jahanzaib, A. Yasmin, I.A. Khan, Pan-genomics, drug candidate mining and ADMET profiling of natural product inhibitors screened against *Yersinia pseudotuberculosis*, *Genomics* 113 (1) (2021) 238–244.
- [33] P. Kavaliuskas, B. Grybaite, V. Mickevicius, R. Petraitiene, R. Grigaleviciute, R. Planciuniene, P. Gialanella, A. Pockevicius, V. Petraitis, Synthesis, ADMET properties, and *in vitro* antimicrobial and antibiofilm activity of 5-nitro-2-thiophenecarbaldehyde N-((E)-(5-nitrothienyl) methylidene) hydrazone (KTU-286) against *Staphylococcus aureus* with defined resistance mechanisms, *Antibiotics* 9 (9) (2020) 612.
- [34] K. Gullapelli, G. Brahmeshwari, M. Ravichander, U. Kusuma, Synthesis, antibacterial and molecular docking studies of new benzimidazole derivatives, *Egypt. J. Basic Appl. Sci.* 4 (4) (2017) 303–309.
- [35] M. Surti, M. Patel, M. Adnan, A. Moin, S.A. Ashraf, A.J. Siddiqui, M. Snoussi, S. Deshpande, M.N. Reddy, Ilimaquinone (marine sponge metabolite) as a novel inhibitor of SARS-CoV-2 key target proteins in comparison with suggested COVID-19 drugs: designing, docking and molecular dynamics simulation study, *RSC Adv.* 10 (62) (2020) 37707–37720.